

Particle acceleration by ion-acoustic solitons in plasma

Hideki Ishihara^{1,*} Ken Matsuno^{1,2,†} Masaaki Takahashi^{3,‡} and Syuto Teramae^{1,§}

¹ *Department of Mathematics and Physics, Graduate School of Science,*

Osaka City University, Sumiyoshi, Osaka 558-8585, Japan

² *Faculty of Health Sciences, Butsuryo College of Osaka, Sakai, Osaka 593-8328, Japan*

and

³ *Department of Physics and Astronomy,*

Aichi University of Education, Kariya, Aichi 448-8542, Japan

Abstract

We propose a new acceleration mechanism for charged particles by using cylindrical or spherical nonlinear acoustic waves propagating in ion-electron plasma. The acoustic wave, which is described by the cylindrical or spherical Kortweg-de Vries equation, grows in its wave height as the wave shrinks to the center. Charged particles confined by the electric potential accompanied with the shrinking wave get energy by repetition of reflections. We obtain power law spectrum of energy for accelerated particles. As an application, we discuss briefly that high energy particles coming from the Sun are produced by the present mechanism.

*Electronic address: ishihara@sci.osaka-cu.ac.jp

†Electronic address: matsuno@sci.osaka-cu.ac.jp

‡Electronic address: mtakahas@aecc.aichi-edu.ac.jp

§Electronic address: teramae@sci.osaka-cu.ac.jp

I. INTRODUCTION

It is known that the energy spectrum of cosmic rays is well described by power laws over a very large energy span [1]. It suggests a nonthermal acceleration mechanism of the high energy particles by a variety of active astrophysical objects: the solar atmosphere, supernova remnants, central region of galaxies, and so on. However, the acceleration mechanisms, which are important to understand the properties of the astrophysical objects, have not yet been elucidated.

One of the most well-studied acceleration mechanisms is the Fermi acceleration [2], where charged particles gain nonthermal energy by repetition of reflections stochastically by magnetic clouds in astrophysical shock waves. By these multiple reflections the resulting energy spectrum of many particles becomes a power law. As alternative possibilities, a lot of mechanisms concerning to magnetic reconnections—double layer, monopole induction, and shock wave (surfing effect), etc.—are studied [3]. We consider a new acceleration mechanism by nonlinear acoustic solitonlike waves excited in a plasma.

We consider a collisionless plasma of cold ions and isothermal electrons. It is well known that the one-dimensional planar ion-acoustic waves in the plasma are governed by the Kortweg-de Vries (KdV) equations [4]. In fact, such waves are really observed experimentally in the plasma system [5].

For cylindrical and spherical ion-acoustic waves in the plasma, modified KdV equations are introduced by Maxon and Viecelli [6, 7], and they showed existence of cylindrical and spherical solitonlike solutions by numerical calculations. While the planar solitons propagate with constant wave heights, the cylindrical and spherical solitons grow in their wave heights during the propagation toward the center. Indeed, these waves are studied by numerical calculations of basic equations describing plasma systems [8, 9], and also observed in laboratories [10, 11].

If the density fluctuation appears in the system of cold ions and warm electrons, the extent of electron density is broader than that of ion density. This means that positive charge excess occurs in the high density region. Therefore, an electric field is produced. The inhomogeneity of density accompanied with the electric field, described by the scalar potential field, propagates as an acoustic wave. Suppose that charged test particles (protons) are confined in the electric potential wall associated with the cylindrical or spherical ion-acoustic waves; the charged particles get energy after some reflections by moving the potential wall as the waves shrink into the center.

An accelerated particle escapes from the potential wall as an output when the energy of the particle exceeds the electric potential energy.

In this paper, we present a new mechanism for the acceleration of charged particles by using nonlinear solitonlike acoustic waves propagating in plasma described by the cylindrical or spherical KdV equation. We show that the power law spectrum for accelerated output particles is obtained. As an application, we briefly discuss a possibility that high-energy particles coming from the Sun are produced by the present acceleration mechanism.

The organization of this paper is as follows. In the next section, we present the basic system considered in this study and derive the modified KdV equation that describes the cylindrically or spherically symmetric ion-acoustic waves. Then, we show the properties of solitonlike solutions to the equation. In Sec. III, we introduce a thin shell wall model to mimic the cylindrical or spherical soliton solution. Using the model, we trace a number of charged test particle motions accelerated by the soliton numerically and obtain the power spectrum of output particles. Section IV is devoted to summary and discussion including an application to the solar cosmic rays.

II. BASIC SYSTEM

A. Basic equations of plasma

We consider a plasma that consists of ions and electrons. The dynamics of the ions is described by a set of equations:

$$Mn^{(i)} \left(\frac{\partial \mathbf{v}^{(i)}}{\partial t} + (\mathbf{v}^{(i)} \cdot \nabla) \mathbf{v}^{(i)} \right) = en^{(i)} (\mathbf{E} + \mathbf{v}^{(i)} \times \mathbf{B}) - \nabla P^{(i)}, \quad (1)$$

$$\frac{\partial n^{(i)}}{\partial t} + \nabla \cdot (n^{(i)} \mathbf{v}^{(i)}) = 0, \quad (2)$$

where $n^{(i)}$, $\mathbf{v}^{(i)}$, $P^{(i)}$ are the number density, the velocity, and the pressure of the ion fluid, and M is the mass of ion. The electric and magnetic fields are denoted by \mathbf{E} and \mathbf{B} , and e is the elementary charge.

We assume that there exists no global magnetic field, and neglect the magnetic field produced by the plasma motion[12]. The electric field \mathbf{E} is described by $\mathbf{E} = -\nabla\phi$, and the electric potential ϕ is governed by the Poisson equation,

$$\Delta\phi = -\frac{e}{\varepsilon_0} (n^{(i)} - n^{(e)}), \quad (3)$$

where $n^{(e)}$ is the number density of electrons, and ε_0 is the vacuum permittivity.

The electrons are assumed to be in thermal equilibrium with the temperature $T^{(e)}$, so that $n^{(e)}$ is given by

$$n^{(e)} = n_0 \exp\left(\frac{e\phi}{k_B T^{(e)}}\right), \quad (4)$$

where k_B is the Boltzmann constant, and n_0 is the homogeneous density of electrons for $\phi = 0$. Furthermore, we consider the case in which $P^{(i)}$ is negligible, namely the ions are cold.

B. Cylindrical KdV and spherical KdV equations

In this paper, we concentrate on nonlinear acoustic waves with cylindrical or spherical symmetry; then the basic equations (1) and (2) are rewritten as

$$\frac{\partial v^{(i)}}{\partial t} + v^{(i)} \frac{\partial v^{(i)}}{\partial r} = -\frac{e}{M} \frac{\partial \phi}{\partial r}, \quad (5)$$

$$\frac{\partial n^{(i)}}{\partial t} + \frac{\partial}{\partial r}(n^{(i)} v^{(i)}) + \frac{2\gamma}{r} n^{(i)} v^{(i)} = 0, \quad (6)$$

and the Poisson equation (3) reduces to

$$\frac{\partial^2 \phi}{\partial r^2} + \frac{2\gamma}{r} \frac{\partial \phi}{\partial r} = -\frac{e}{\varepsilon_0} \left(n^{(i)} - n_0 \exp\left(\frac{e\phi}{k_B T^{(e)}}\right) \right), \quad (7)$$

where $\gamma = 1/2$ for the cylindrical case, and $\gamma = 1$ for the spherical case, respectively. The independent variable r is the radial coordinate in the cylindrical or spherical coordinate system.

For the purpose of taking acoustic waves that shrink toward the center into consideration, according to the reductive perturbation method [4], we introduce new variables

$$\xi = \frac{\epsilon^{1/2}}{\lambda_D} (r + c_0 t), \quad (8)$$

$$\tau = \frac{\epsilon^{3/2}}{\lambda_D} c_0 t, \quad (9)$$

where ϵ is a small constant, λ_D is the Debye length given by

$$\lambda_D = \sqrt{\frac{\varepsilon_0 k_B T^{(e)}}{n_0 e^2}}, \quad (10)$$

and c_0 is the sound velocity defined by

$$c_0 = \sqrt{\frac{k_B T^{(e)}}{M}}. \quad (11)$$

We rewrite Eqs.(5)-(7) with these variables as

$$\epsilon^{1/2}c_0\frac{\partial v^{(i)}}{\partial \xi} + \epsilon^{3/2}c_0\frac{\partial v^{(i)}}{\partial \tau} + \epsilon^{1/2}v^{(i)}\frac{\partial v^{(i)}}{\partial \xi} = -\epsilon^{1/2}\frac{e}{M}\frac{\partial \phi}{\partial \xi}, \quad (12)$$

$$\epsilon^{1/2}c_0\frac{\partial n^{(i)}}{\partial \xi} + \epsilon^{3/2}c_0\frac{\partial n^{(i)}}{\partial \tau} + \epsilon^{1/2}\frac{\partial}{\partial \xi}(n^{(i)}v^{(i)}) - \epsilon^{3/2}\frac{2\gamma}{(\tau - \epsilon\xi)}n^{(i)}v^{(i)} = 0, \quad (13)$$

$$\epsilon\frac{\partial^2 \phi}{\partial \xi^2} - \epsilon^2\frac{2\gamma}{(\tau - \epsilon\xi)}\frac{\partial \phi}{\partial \xi} = -\lambda_D^2\frac{e}{\epsilon_0}\left(n^{(i)} - n_0 \exp\left(\frac{e\phi}{k_B T^{(e)}}\right)\right). \quad (14)$$

We expand variables $v^{(i)}$, ϕ and $n^{(i)}$ by ϵ in the form

$$\frac{v^{(i)}}{c_0} = \epsilon v_1 + \epsilon^2 v_2 + \dots, \quad (15)$$

$$\frac{e\phi}{k_B T^{(e)}} = \epsilon \phi_1 + \epsilon^2 \phi_2 + \dots, \quad (16)$$

$$\frac{n^{(i)}}{n_0} = 1 + \epsilon n_1 + \epsilon^2 n_2 + \dots. \quad (17)$$

Substituting Eqs.(15)-(17) into Eqs.(12)-(14), we obtain a set of equations order by order in ϵ . The lowest equations in ϵ are

$$n_1 = -v_1 = \phi_1, \quad (18)$$

and the second lowest order equations give

$$\frac{\partial n_1}{\partial \tau} - \frac{\partial v_1}{\partial \tau} - v_1 \frac{\partial v_1}{\partial \xi} + \phi_1 \frac{\partial \phi_1}{\partial \xi} + \frac{\partial}{\partial \xi}(n_1 v_1) - \frac{\partial^3 \phi_1}{\partial \xi^3} - 2\gamma \frac{v_1}{\tau} = 0. \quad (19)$$

From Eqs.(18) and (19) we obtain

$$\frac{\partial \Phi}{\partial \tau} - \Phi \frac{\partial \Phi}{\partial \xi} - \frac{1}{2} \frac{\partial^3 \Phi}{\partial \xi^3} + \gamma \frac{\Phi}{\tau} = 0, \quad (20)$$

where $\Phi := \phi_1 = -v_1 = n_1$. If $\gamma = 0$, Eq.(20) is the KdV equation, which describes nonlinear plane waves. In the case $\gamma = 1/2$ or 1 the equation is the extended KdV equation that describes cylindrical or spherical waves, respectively. From Eqs.(8) and (9) we see

$$r = \lambda_D(\epsilon^{-1/2}\xi - \epsilon^{-3/2}\tau), \quad (21)$$

then $r = 0$ corresponds to $\tau = 0$ in the lowest order with respect to ϵ . The cylindrical or spherical wave shrinks from an initial radius $r = r_0$ to $r = 0$ as increasing τ from the initial time $\tau = \tau_0 < 0$ to $\tau = 0$.

C. Properties of cylindrical and spherical soliton solutions

We study characteristic properties of solitonlike wave solutions with cylindrical or spherical symmetry. In the case of $\gamma = 0$, it is well known that the KdV equation has soliton solutions in

the form

$$\Phi = A \operatorname{sech}^2 \left[\sqrt{\frac{A}{6}} \left(\xi + \frac{A}{3} \tau \right) \right], \quad (22)$$

where the wave height denoted by A is a constant. The soliton described by the solution (22) propagates with the constant velocity $A/3$ in the ξ - τ plane, keeping its shape invariant.

In the cylindrical or spherical case, $\gamma = 1/2$ or 1 , we set a wave with the radius $r = r_0$ and the width is much smaller than r_0 at the initial time. In this set up, the cylindrical or spherical wave is described approximately by the planar wave Eq.(22). However, the wave height is no longer constant owing to the existence of the last term in Eq.(20). As is shown later, the wave height grows in time as the wave shrinks toward the center. Numerical solutions to the cylindrical KdV and the spherical KdV equations are widely studied [6, 7, 13–15] and showed the growth of the wave height.

For a wave on a finite support, Eq.(20) admits a conserved quantity Q in the form

$$Q = |\tau|^{2\gamma} \int_{-\infty}^{\infty} \Phi^2 d\xi. \quad (23)$$

After replacing the constant A in Eq.(22) by a function $A(\tau)$ we substitute it into Eq.(23), then we see the peak height of the waves grows as $(\tau/\tau_0)^{-4\gamma/3}$ while the width shrinks as $(\tau/\tau_0)^{2\gamma/3}$ [13].

In the final stage, $\tau \sim 0$, of the cylindrical case, $\gamma = 1/2$, we find that the time derivative term and the time dependent term, the first and the last terms, dominate the nonlinear term and the dispersive term, the second and third terms, in Eq.(20) for a wide range of initial conditions of numerical calculations. Namely, Eq.(20) becomes

$$\frac{\partial \Phi}{\partial \tau} + \frac{1}{2} \frac{\Phi}{\tau} \approx 0, \quad (24)$$

then we see that the wave height grows as $\sim (\tau/\tau_0)^{-1/2}$ with a constant width. On the other hand, in the final stage of the spherical case, $\gamma = 1$, for numbers of initial conditions, we observe numerically that the contribution of the dispersive term becomes small, and the wave height grows as $\sim (\tau/\tau_0)^{-1}$. Figure 1 and Figure 2 show the numerical evolution of the wave forms of cylindrical and spherical solitons. Figure 3 shows examples of the time dependence of the wave height in both cases.

The amplitude $\Phi = \phi_1$ of the wave describes the electric potential produced by the charge excess at the peak of the wave. The cylindrical or spherical wave is accompanied by the cylindrical or spherical electric potential wall. We consider test charged particles that are confined by the

potential wall. The moving charged particles are reflected by the shrinking potential wall, and the particles are accelerated. When the particle gets kinetic energy greater than the electric potential, the particle escapes from the region enclosed by the potential wall. The wave height of the cylindrical or spherical wave grows as the wall shrinks toward the center, the energy spectrum of escaped particles depends on the time evolution of the wave height.

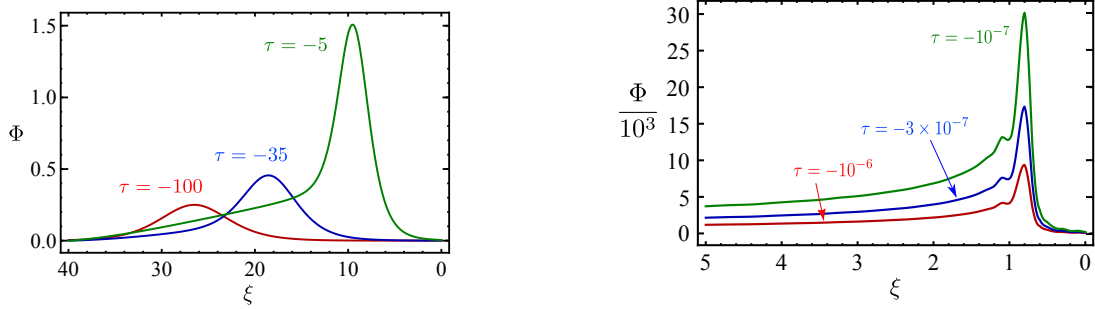


FIG. 1: Evolution of the cylindrical soliton. Wave forms in the early stage: $\tau = -100, -35, -5$ (left panel). Wave forms in the final stage: $\tau = -10^{-6}, -3 \times 10^{-7}, -10^{-7}$ (right panel).

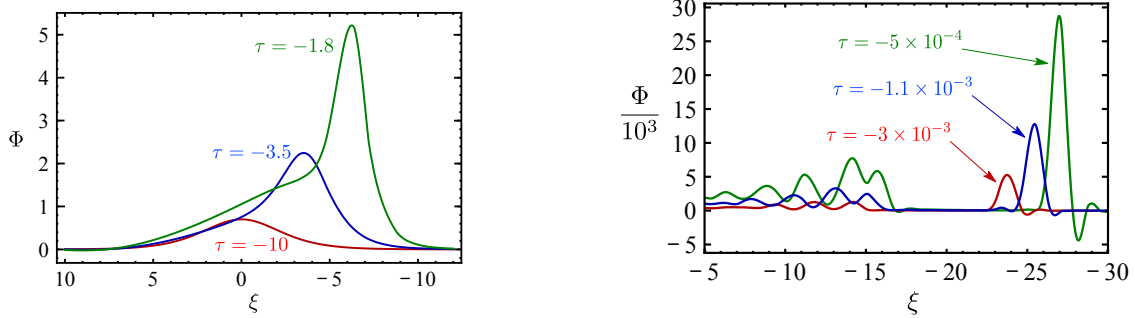


FIG. 2: Evolution of the spherical soliton. Wave forms in the early stage: $\tau = -10, -3.5, -1.8$ (left panel). Wave forms in the final stage: $\tau = -3 \times 10^{-3}, -1.1 \times 10^{-3}, -5 \times 10^{-4}$ (right panel).

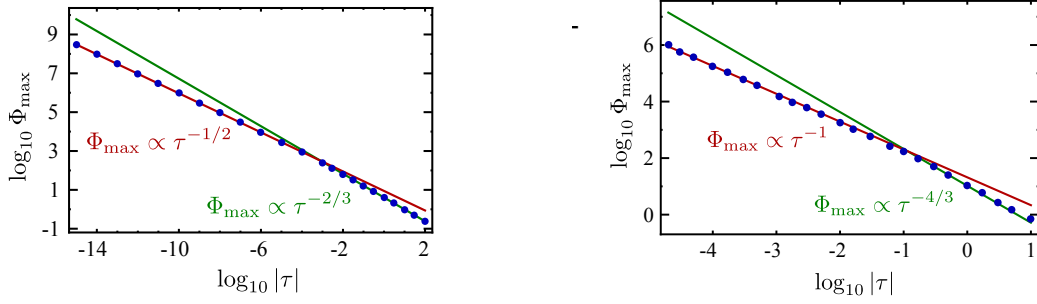


FIG. 3: Time evolution of the wave height Φ_{\max} for the cylindrical soliton (left panel). In the early stage $\Phi_{\max} \propto \tau^{-2/3}$, while in the final stage $\Phi_{\max} \propto \tau^{-1/2}$. The same one for the spherical soliton (right panel). In the early stage $\Phi_{\max} \propto \tau^{-4/3}$, while in the final stage $\Phi_{\max} \propto \tau^{-1}$.

III. ACCELERATION OF PARTICLES

We consider that test charged particles are accelerated by the shrinking potential wall described by the cylindrical or spherical solitons. In order to simplify the system, we make a model that the soliton is replaced by a thin shell wall. We calculate test particle motion enclosed by this shrinking thin shell wall numerically and obtain the energy spectrum of the accelerated particles.

A. Thin shell wall models

In contrast to the plane soliton solution to the KdV equation, the most important property of the cylindrical or spherical soliton is that the wave height grows in time, t , as the wave goes to the center. We reduce the cylindrical or spherical soliton to a thin shell wall at the peak position of the wave, where the width of the wave is ignored. Furthermore, we ignore, here, the motion of the wave in the ξ - τ plane. It means that the wave propagates with the speed c_0 in the r - t plane. The thin shell wall describes the electric potential wall whose height evolves in time.

The model of the thin shell wall is specified by the following properties:

1. The initial radius of the shell is r_0 at the initial time $t_0 (< 0)$. We assume the speed of thin shell in the r - t plane is the sound speed c_0 , then the radius of the shell is described by $r(t) = -c_0 t$.

2. According to the growth rate of the wave height of the cylindrical or spherical soliton discussed in the previous section, we assume that the height of the thin shell wall grows as $\Phi(t) = \Phi_0 (t/t_0)^{-\alpha}$, $\alpha = 1/2$ or $2/3$ for the cylindrical case, and $\alpha = 1$ or $4/3$ for the spherical case, where Φ_0 is the initial amplitude of electric potential.
3. We should stop the thin shell wall evolution when the shell radius becomes the Debye length. Then the final time is given by $t_f = -\lambda_D/c_0$.

Motion of test charged particles is assumed as follows:

1. *Elastic reflection*

A moving charged particle toward the thin shell wall with the velocity $\mathbf{v} = (v_\perp, v_\parallel)$ gets the velocity $\mathbf{v} = (-v_\perp - 2c_0, v_\parallel)$ after a reflection by the shrinking wall with the sound velocity c_0 , where v_\perp and v_\parallel are the velocity components of the normal and tangential to the thin shell wall, respectively.

2. *Collisionless*

We assume that each charged test particle moves with a constant velocity till it hits the thin shell wall, and the test particles do not collide with each other.

3. *Particle escaping criterion*

If the kinetic energy of a particle exceeds the height of the thin shell wall $\Phi(t)$, the wall cannot confine the particle then the particle escapes to the infinity as an output particle.

A typical trajectory of a test particle reflected by the shrinking thin shell wall is shown in Fig.4.

B. Numerical studies for acceleration of particles

We consider protons as ions, i.e., M is the proton mass M_P , and settle a thin shell wall initially with $r_0 = 10^6 \lambda_D$ and $\Phi_0 = k_B T^{(e)}$. The initial time and final time are given by $t_0 = -r_0/c_0$ and $t_f = -\lambda_D/c_0$, where the sound velocity c_0 is given by Eq.(11).

Here, we consider the initial distribution of the test charged particles. We assume the Maxwell distribution with the temperature $T \leq T^{(e)}$ of test charged particles with a constant spatial density enclosed by the thin shell wall (see Fig.5).

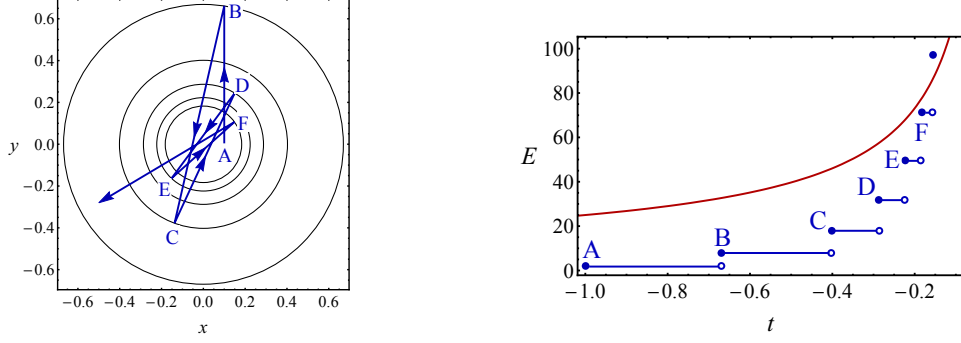


FIG. 4: A typical trajectory of a test particle in the cylindrical case (left panel). The particle is reflected elastically by the shrinking thin shell. Time evolution of electric potential, $\Phi \propto t^{-2/3}$, is drawn by the solid (red) curve, and particle energy gained by reflections is shown by bars (right panel).

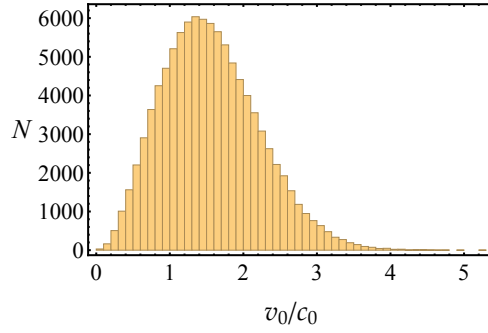


FIG. 5: Initial distribution function of 10^5 test charged particles is assumed to be the Maxwell distribution.

We trace a number of test particles moving and reflected by the thin shell wall, and obtain the energy spectrum of output particles in $\alpha = 2/3$ and $\alpha = 1/2$ in the cylindrical case, and $\alpha = 4/3$ and $\alpha = 1$ in the spherical case. Figure 6 and Figure 7 show that the high-energy part of the energy spectrum is described by a power law, E^{-p} , in these models. Table I shows that the values of power index $-p$ for different α and several initial temperatures of the test particles T . In both cylindrical and spherical models, the power index $-p$ depends on α , which determines the evolution of the electric potential height. However, it does not depend on the temperature of initial distribution of the test charged particles.

In the numerical experiments with 10^5 initial test particles, the maximum energy of the output

particle is $3.8 \times 10^2 k_B T^{(e)}$ for $\alpha = 2/3$, and $5.1 \times 10 k_B T^{(e)}$ for $\alpha = 1/2$ in the cylindrical model. The same one is $4.2 \times 10^6 k_B T^{(e)}$ for $\alpha = 4/3$, and $2.1 \times 10^3 k_B T^{(e)}$ for $\alpha = 1$ in the spherical model. All particles escape from the thin shell wall before $t = t_f$ in the present calculations. The power law spectrum of the output particles, which does not depend on the initial numbers of particles, has no characteristic scale of energy; then if we set much numbers of test particles initially, we can get more energetic output particles. The maximum energy is limited by the applicability of the soliton model. Particles can be accelerated till the radius of cylindrical or spherical solitons become the Debye length. Therefore, if the initial numbers of particles is large enough, we would obtain the energy $E_{max} = \Phi(t_f)$ as the maximum.

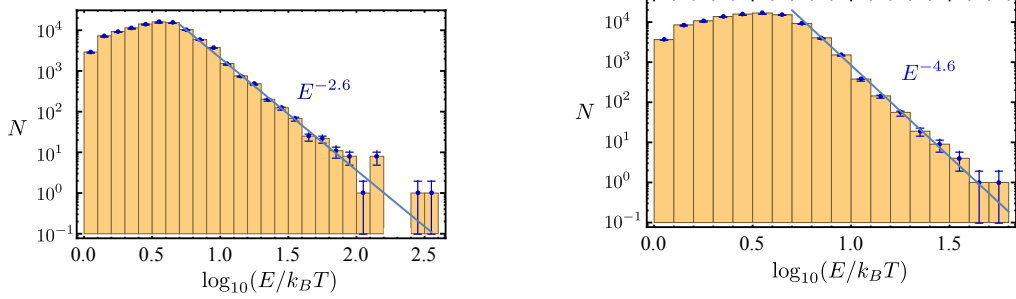


FIG. 6: Energy spectrum of output particles in the cylindrical model. The case of $\alpha = 2/3$ (left panel), and the case of $\alpha = 1/2$ (right panel).

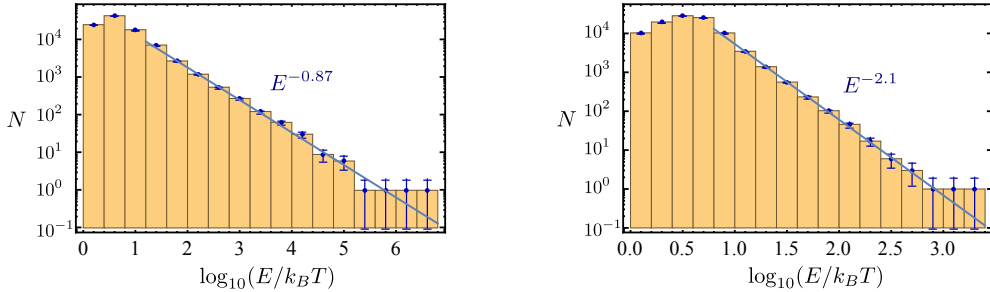


FIG. 7: Energy spectrum of output particles in the spherical model. The case of $\alpha = 4/3$ (left panel), and the case of $\alpha = 1$ (right panel).

TABLE I: Power indices: The thin shell wall models are characterized by the index α , where the wave height is described as $\Phi = \Phi_0(t/t_0)^{-\alpha}$. Energy spectra of the output particles are given by E^{-p} .

Cylindrical model:

	$T/T^{(e)} = 0.1$	$T/T^{(e)} = 0.5$	$T/T^{(e)} = 1.0$
$\alpha = 2/3$	$p = 2.5$	$p = 2.5$	$p = 2.6$
$\alpha = 1/2$	$p = 4.9$	$p = 4.4$	$p = 4.6$

Spherical model:

	$T/T^{(e)} = 0.01$	$T/T^{(e)} = 0.1$	$T/T^{(e)} = 1.0$
$\alpha = 4/3$	$p = 0.84$	$p = 0.84$	$p = 0.87$
$\alpha = 1$	$p = 2.1$	$p = 2.0$	$p = 2.1$

To clarify which part of energy in initial particle distribution contributes the output energy spectrum, we divide initial particles into three groups:

$$(i) \ E \leq \Phi_0/2 \quad (v_0 \leq \sqrt{\Phi_0/M}), \quad (25)$$

$$(ii) \ \Phi_0/2 < E \leq \Phi_0 \quad (\sqrt{\Phi_0/M} < v_0 \leq \sqrt{2\Phi_0/M}), \quad (26)$$

$$(iii) \ \Phi_0 < E \quad (\sqrt{2\Phi_0/M} < v_0), \quad (27)$$

by the initial kinetic energy (see Fig. 8). In the spherical model with $\alpha = 4/3$, we calculate acceleration of particles and obtain the output energy spectrum as shown in Fig. 9. We can see that the lowest energy group (i) contributes the higher part of the output energy spectrum. Since the particles with higher energy than Φ_0 cannot be trapped by the thin shell wall, then the particles in higher initial energy group (iii) are not accelerated effectively. Further, we find that low initial energy groups (i) and (ii) make some peaks in lower range of the output energy with interval $\Delta(v/c_0) \sim 2$. The particles gain the velocity by $2c_0$ for each reflection; then these peaks correspond to the numbers of reflections of test particles by the shrinking shell with the speed c_0 .

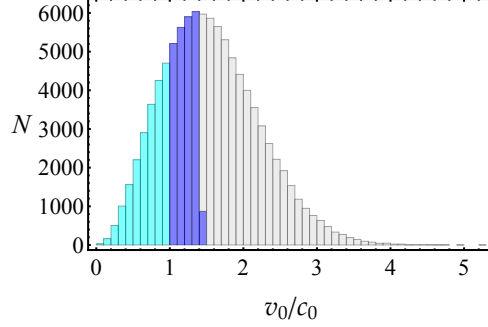


FIG. 8: Initial particles are classified into three groups by energy: (i) $E \leq \Phi_0/2$ (light blue), (ii) $\Phi_0/2 < E \leq \Phi_0$ (dark blue), (iii) $\Phi_0 < E$ (gray).

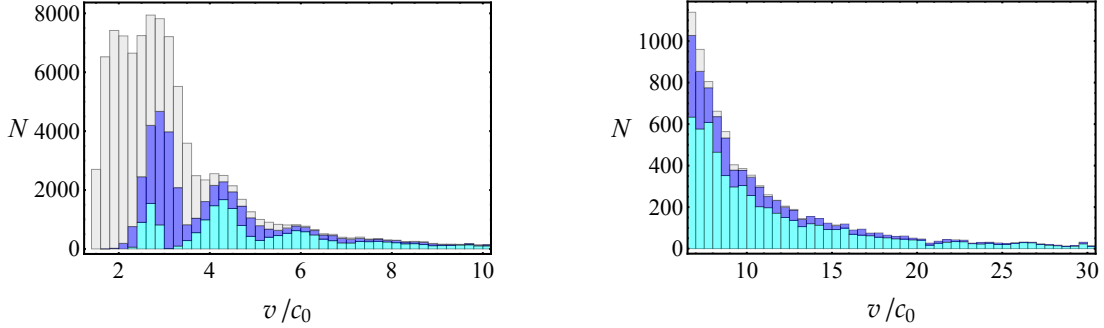


FIG. 9: Energy distribution of output particles. Particles in groups (i) and (ii) make peaks with the interval $\Delta(v_0/c_0) \sim 2$ (left panel). High energy part of distribution is shown in the right panel. Almost particles in the high energy part consist of the groups (i) and (ii).

IV. SUMMARY AND DISCUSSION

We have investigated a new acceleration mechanism, soliton acceleration, for charged particles by using cylindrical or spherical nonlinear acoustic waves propagating in the plasma that consists of cold ions and warm electrons. We have shown that power law spectra for accelerated output particles are obtained.

The proposed mechanism is different from the Fermi acceleration in the following two points. First, in contrast to the Fermi acceleration, where the charged particles are accelerated by stochastic reflections by magnetic clouds, in the soliton acceleration, the particles are accelerated deterministically in a cylindrical or spherical electric potential wall that shrinks with an acoustic soliton. In both mechanisms, the power law of energy spectrum of accelerated particles is obtained. The

reason for the power law in the Fermi acceleration is stochasticity; while in the soliton acceleration, the reason is that the growth rate of the wave height is the power law in time.

Secondly, in the Fermi acceleration, only particles with energies that exceed the thermal energy by much can cross the shock and can be accelerated. It is not clear what mechanism causes the initial particles to have energies sufficiently high. This is the so-called “injection problem”. However, particles with the energy less than the initial electric potential energy are accelerated effectively in the soliton acceleration. Therefore there is no injection problem in the present mechanism.

We expect that the soliton acceleration mechanism presented in this article can apply to the high energy protons of cosmic rays. For example, we try to apply to the high energy protons coming from the Sun. The high energy protons with the energy range from MeV to GeV are observed when the solar flare occurs [16]. The solar flare is an energetic electromagnetic phenomenon in a short time scale. It is widely considered that reconnection of the magnetic field lines occurs during solar flare activities [3]. In the magnetic reconnection region, where the footpoint region of the flare at the chromosphere is, the plasma density decreases by coronal mass ejection, and the magnetic field becomes negligibly small. The cylindrical or spherical solitons of ion-acoustic waves with the size of reconnection region would be excited there [17]. Here, we ignore the magnetic field and plasma bulk flow.

We set the temperature of the solar plasma as $T_{\odot}^{(e)} = 1 \sim 100\text{eV}$, and the number density of electrons as $n_0 = 10^{15} \sim 10^{16}\text{m}^{-3}$, then the Debye length as $\lambda_D = 10^{-4} \sim 10^{-3}\text{ m}$, and the sound velocity $c_0 = 10^4 \sim 10^5\text{ m/sec}$ for a flare region in the solar atmosphere. The radius of the initial wave is assumed to be the size of the reconnection region: $r_0 = 10^4\text{m} = 10^7 \sim 10^8\lambda_D$ [17]. The time scale of the soliton acceleration is given by the initial radius of the wave divided by the speed of the wave, namely $10^{-1} \sim 1\text{ sec}$. We assumed that the injection energy of the particles is of the same order as the thermal energy of the solar atmosphere, i.e., $k_B T_{\odot}^{(e)}$.

According to the numerical calculation by the shell models in the previous section, the output energy spectrum is power law E^{-p} with the index $p = 2.5 \sim 4.9$ for the cylindrical model, and $p = 0.8 \sim 2.1$ for the spherical model (see Table I). If the model is applicable till the cylindrical or spherical shell wall shrinks to the size of Debye length, the maximum energy is estimated as

$$E_{\text{max}} \approx \Phi_0 \left(\frac{t_f}{t_0} \right)^{-\alpha} = k_B T_{\odot}^{(e)} \left(\frac{r_0}{\lambda_D} \right)^{\alpha} \approx 2\text{ GeV} \sim 5\text{ TeV}, \quad (28)$$

where the number of input particles is assumed to be large enough. Our model would be a candidate

for origin of the solar cosmic rays energetically.

We have found that the growth rate of the wave height of a soliton changes in time from the initial stage to the final stage (see Fig.3). If we take the change of growth rate into account, we can consider hybrid shell models, i.e.,

Cylindrical shell model,

$$\text{initially : } \Phi \propto (t/t_0)^{-2/3}; \quad \text{finally : } \Phi \propto (t/t_0)^{-1/2}, \quad (29)$$

Spherical shell model,

$$\text{initially : } \Phi \propto (t/t_0)^{-4/3}; \quad \text{finally : } \Phi \propto (t/t_0)^{-1}, \quad (30)$$

to the solar cosmic rays. In the hybrid models, we obtain the energy spectrum shown in Fig. 10. If the double power law reported in Ref.[16] should be explained by the acceleration mechanism, the soliton acceleration, which leads the double power law naturally, would be a hopeful candidate.

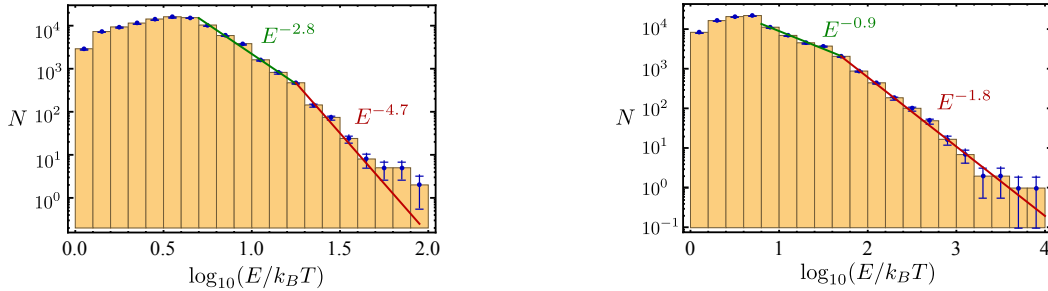


FIG. 10: Double power spectrum in the cylindrical shell model (left panel). The power indices $p = 2.8$ in the low energy side and $p = 4.7$ in the high energy side. The same one in the spherical shell model (right panel). The power indices $p = 0.9$ in the low energy side and $p = 1.8$ in the high energy side.

The maximum value of output energy (28) exceeds the observed value of solar cosmic rays [16]. In realistic cases, the final size of the wave would be much larger than the Debye length, and the KdV description, which is obtained by the reductive perturbation method for weakly nonlinear waves, would break down due to the full nonlinearity of the waves in the final stage. We have used the solution of the KdV equation to the highly nonlinear stage in this work in order to understand fundamental properties of the particle acceleration mechanism. One of the necessary properties

for the acceleration mechanism by the waves with the electric potential is growth of the amplitude with a power law in time as the waves shrink. To explain the observed data of the solar cosmic rays, it is important to investigate the fully nonlinear solutions for the ion-acoustic wave rather than the weakly nonlinear wave solution described by the KdV equation [18].

The soliton acceleration mechanism presents the source of high energy particles at a footpoint of a solar flare. To explain observed data of the solar cosmic rays, we should consider the escape process of the high energy particles from the solar atmosphere, and the propagation process toward a detector on the earth, and so on. These processes would reduce the energy and modify the spectrum of particles produced by the mechanism. However, the discussion of these processes is beyond the scope of this article.

In this work, we neglect the magnetic field for simplicity. In most astrophysical phenomena the magnetic field plays important roles. It would be possible to generalize the soliton acceleration mechanism proposed in this paper in the environment of nonvanishing magnetic field. We will study this issue in the next work.

Acknowledgment

The authors would like to thank Dr. Ken-ichi Nakao, Dr. Hiromitsu Hamabata, and Dr. Youhei Masada for valuable discussions. H.I. was supported by JSPS KAKENHI Grant Number 16K05358. M.T. was supported by JSPS KAKENHI Grant Number 17K05439, and DAIKO FOUNDATION.

-
- [1] T. K. Gaisser, R. Engel, and E. Resconi, *Cosmic Rays and Particle Physics* (Cambridge University Press, Cambridge, England, 1991).
 - [2] E. Fermi, Phys. Rev. **75**, 1169 (1949).
 - [3] M. Aschwanden, *Physics of the Solar Corona* (Springer Press, Berlin, Germany, 2005).
 - [4] H. Washimi and T. Taniuti, Phys. Rev. Lett. **17**, 996 (1966).
 - [5] H. Ikezi, R.J. Taylor, and D.R. Baker, Phys. Rev. Lett. **25**, 11 (1970).
 - [6] S. Maxon and J. Viecelli, Phys. Fluids **17**, 1614 (1974).
 - [7] S. Maxon and J. Viecelli, Phys. Rev. Lett. **32**, 4 (1974).
 - [8] T. Ogino and S. Takeda, J. Phys. Soc. Jpn. **41**, 257 (1976).

- [9] T. E. Sheridan, Phys. Plasmas **24**, 092303 (2017).
- [10] N. Hershkowitz and T. Romesser, Phys. Rev. Lett. **32**, 581 (1974).
- [11] F. Ze, N. Hershkowitz, C. Chan, and K. E. Lonngren, Phys. Fluids **22**, 1554 (1979).
- [12] Particle acceleration by wave packets of magnetohydrodynamic waves is discussed in Y. Kuramitsu and T. Hada, Geophys. Res. Lett. **27**, 629 (2000).
- [13] K. Ko and H. H. Kuehl, Phys. Fluids **22**, 1343 (1979).
- [14] Y. Hase, S. Watanabe, and H. Tanaca, J. Phys. Soc. Jpn. **54**, 4115 (1985).
- [15] E. Infeld and G. Rowlands, *Nonlinear Waves, Solitons and Chaos* (Cambridge University Press, Cambridge, England, 2000).
- [16] R. A. Mewaldt *et al.*, J. Geophys. Res. **110**, A09S18 (2005).
- [17] M.T. Song, S.T. Wu, and M. Dryer, Astrophys. Space Sci. **152**, 287 (1989).
- [18] G. M. Webb, R. H. Burrows, X. Ao, and G. P. Zank, J. Plasma Phys. **80**, 147 (2014).